



HAL
open science

Towards a grain-scale modeling of crack initiation in rolling contact fatigue - Part 1: Shear stress considerations

Lucas Fourel, Jean-Philippe Noyel, Etienne Bossy, Xavier Kleber, Philippe Sainsot, Fabrice Ville

► To cite this version:

Lucas Fourel, Jean-Philippe Noyel, Etienne Bossy, Xavier Kleber, Philippe Sainsot, et al.. Towards a grain-scale modeling of crack initiation in rolling contact fatigue - Part 1: Shear stress considerations. Tribology International, 2021, 164, pp.107224. 10.1016/j.triboint.2021.107224 . hal-03483019

HAL Id: hal-03483019

<https://hal.science/hal-03483019v1>

Submitted on 8 Jul 2022

HAL is a multi-disciplinary open access archive for the deposit and dissemination of scientific research documents, whether they are published or not. The documents may come from teaching and research institutions in France or abroad, or from public or private research centers.

L'archive ouverte pluridisciplinaire **HAL**, est destinée au dépôt et à la diffusion de documents scientifiques de niveau recherche, publiés ou non, émanant des établissements d'enseignement et de recherche français ou étrangers, des laboratoires publics ou privés.



Distributed under a Creative Commons Attribution - NonCommercial 4.0 International License

Towards a Grain-scale Modeling of Crack Initiation in Rolling Contact Fatigue - Part 1: Shear Stress Considerations

Lucas Fourel^{a,b,c}, Jean-Philippe Noyel^b, Etienne Bossy^b, Xavier Kleber^c, Philippe Sainsot^a and Fabrice Ville^{a,*}

^aUniv Lyon, INSA Lyon, CNRS, LaMCoS, UMR5259, 69621 Villeurbanne, France

^bUniv Lyon, ECAM Lyon, LabECAM, F-69005 Lyon, France

^cUniv Lyon, INSA Lyon, MATEIS, UMR CNRS 5510, F-69621 Villeurbanne, France

ARTICLE INFO

Keywords:

Rolling contact

Fatigue

Mesoscopic

Numerical analysis

ABSTRACT

A numerical model for rolling contact fatigue has been developed using finite element method and the Tanaka-Mura micromechanical model to calculate fatigue crack threshold. Two different approaches are compared: macroscopic modeling and mesoscopic modeling which considers a Voronoi polycrystalline geometry. Smooth and dented surface contacts are considered and different methods for computing shear stress are compared. It is shown that a mesoscopic length scale consideration offers benefits over a macroscopic approach in the case of dented surface meanwhile orthogonal shear stress computation on the macroscopic model can legitimately be used in the case of Hertzian contact. The article also highlights that mesoscopic modeling allows for life scatter on fatigue crack threshold. Initiation depths are consistent with literature experiments.

1. Introduction

In many engineering applications, fatigue is the primary failure mechanism that governs the life of a component. During the 19th century, it was thought that the sudden failure of metal railway axles was due to the crystallization of the metal, but this lead quickly gave way to another theory: fatigue. In 1870, Wöhler summarized his work on railroad axles. He concludes that cyclic stress range is more important than peak stress and introduces the concept of endurance limit [1]. Since then, numerous experiments and studies have investigated this mechanism of failure. Basquin (1910) [2], Palmgren and Miner (1945) [3, 4], Coffin and Manson (1954) [5, 6] proposed rules to predict the number of cycles prior to fatigue failure based on stress-life or strain-life relationships.

Rolling Contact Fatigue (RCF) refers to parts that are subjected to repeated contact pressure such as rolling bearings or gears. RCF is characterized by the initiation of a subsurface micro-crack and results in irreversible surface damages such as micropitting, wear or spalling [7]. In order to predict the service life of these components and to understand the mechanisms causing their failure, empirical and numerical models were developed. Many of them are described in Sadeghi's review [8]. However, there is currently no complete predictive life model, and understanding RCF failure mechanism remains a significant challenge. RCF is characterized by multiple damage stages: crack initiation, crack propagation and material failure [9]. Microstructure is known as having an important role especially in the first two stages [10].


In 1981, Tanaka and Mura proposed a micromechanical model for crack initiation [11]. Recent studies have proposed

implementations of the Tanaka-Mura law in mesoscopic numerical model using Voronoi tessellations. Bruckner-Foit et al. [12, 13] studied the fatigue crack threshold on martensitic steel and Toyoda et al. [14] on thin-walled high strength steel. Hilgendorff et al. [15] used boundary element method to compute stress field and Briffod et al. [16] investigated crack initiations in pure iron aggregate. They all use numerical methods for stress computation combined with the Tanaka-Mura model for fatigue crack initiation. However, these works only cover uniaxial loading conditions. Zhou et al. [17, 18] and Cheng et al. [19, 20] have applied Tanaka-Mura's law to RCF, although they used analytical methods for computing the stress field which restricted the studies to Hertzian contact conditions. Other researchers used Voronoi tessellations in RCF combined with continuum damage mechanics [21, 22, 23], the Dang-Van criterion [24, 25] or Fatemi-Socie criterion [26] to predict crack initiation. Some studies also considered competition between surface and subsurface initiated failure due to complex contact conditions in RCF [27, 28].

In this study, the Tanaka-Mura model is used in combination with finite element method (FEM) which allows for moving contact pressures with complex contact conditions such as a dented surface. But rough surfaces or ElastoHydroDynamics (EHL) lubrication could also be considered. A microstructure is randomly generated by a Voronoi tessellation.

The first part of this article will describe the Tanaka-Mura model and material properties. The second part will detail a macroscopic approach which is utilized to study the influence of the different shear stresses, including orthogonal and maximum shear stresses which are often discussed. The final part will detail a mesoscopic approach which takes advantage of the polycrystalline geometry and grain size and distribution.

*Corresponding author

 fabrice.ville@insa-lyon.fr (F. Ville)

ORCID(s): 0000-0002-9743-8820 (F. Ville)

Nomenclature

Δp_{dent}	Dent contribution to contact pressure [Pa]
$\Delta \tau$	Shear stress range [Pa]
ν	Poisson's ratio
ϕ	Dent diameter [m]
σ_x	Normal stress in x direction [Pa]
σ_y	Normal stress in y direction [Pa]
σ_z	Normal stress in z direction [Pa]
τ_{45}	Orthogonal shear stress rotated by 45° from xy direction [Pa]
τ_{max}	Maximum shear stress [Pa]
τ_{meso}	Mesosopic shear stress [Pa]
τ_{oct}	Octahedral shear stress [Pa]
τ_{xy}	Orthogonal shear stress in xy direction [Pa]
A	Material constant
a	Contact half-width [m]
B	Material constant
d	Slip band length [m]
d_{th}	Dent depth [m]
E	Young modulus [Pa]
G	Shear modulus [Pa]
k	Frictional stress [Pa]
N_i	Fatigue crack threshold
p	Contact pressure [Pa]
p_0	Maximum Hertz contact pressure [Pa]
p_{hertz}	Hertz contact pressure [Pa]
u_x	Displacement in x direction [m]
u_y	Displacement in y direction [m]
W_s	Fracture energy [J/m^2]

2. Fatigue predictive modeling

Sadeghi et al. [8] reviewed the different probabilistic engineering life models for RCF like the Lundberg-Palmgren [29] and Ioannides-Harris [30] theories. These early works are based on empirical results and propose formulas to calculate the fatigue life of classical components such as rolling bearings. In Sadeghi's review [8], deterministic research life models for RCF are also presented. These models are based on the physical principles of failure. Different types of models have been originally developed to compute the fatigue lives: models which focus on crack initiation and models which focus on crack propagation. The model used in this study is the Tanaka-Mura law. It is based on the micromechanics of fatigue crack initiation and can be easily implemented under its stress-life relationship form. Tanaka and Mura created their micromechanical model in 1981. It predicts the fatigue crack threshold based on the accumulation of dislocations in Persistent Slip Bands (PSBs) [11]. It uses the energy balance of the dislocation structure along the PSB which can lead to crack initiation after a certain number of loading cycles [31].

The Tanaka-Mura model does not consider normal stress but only shear stress. In addition, in the energy balance some simplifications are made concerning the hysteresis loop. Improvements of the model have been suggested by Mura and Nakasone [32, 33] which proposed using Gibb's free energy. Other authors offered variants of this model with the use of additional parameters such as the Burgers vector [34] or the PSB width [35]. The original model has nevertheless received a great popularity within the scientific community because it captures the essence of crack initiation via slip and accumulation of dislocations. The Tanaka-Mura model is consistent with three fundamental fatigue concepts [36]:

- The Manson-Coffin [6, 5] empirical equation where the fatigue life is inversely proportional to the square of the plastic strain amplitude
- The Hall-Petch [37, 38] relation between the grain size and the high-cycle fatigue
- The Palmgren-Miner [3, 4] law of damage accumulation for loads with variable amplitudes

Several studies were able to correlate the Tanaka-Mura fatigue crack initiation model with experimental results [13, 36, 39, 40]. Cheng and Cheng compared the model to experiments in the case of contact fatigue [19, 20].

The number of cycles required to initiate a crack is described in Equation 1.

$$N_i = \frac{8GW_s}{\pi(1-\nu)d(\Delta\tau - 2k)^2} \quad (1)$$

- G Shear modulus, [Pa]
- W_s Fracture energy, [J/m^2]
- ν Poisson's ratio, [-]
- d Slip band length, [m]
- $\Delta\tau$ Shear stress range, [Pa]
- k Frictional stress, [Pa]

Tanaka-Mura equation can be simplified as:

$$N_i = \frac{A}{d(\Delta\tau - B)^2} \quad (2)$$

Using A and B as material constants:

$$A = \frac{8GW_s'}{\pi(1-\nu)} \quad (3)$$

$$B = 2k \quad (4)$$

Different values of the material properties can be found in the literature, therefore, Table 1 compiles ranges given for bearing steels [13, 14, 15, 36, 39, 40].

Table 1
Ranges of material properties.

Property	Minimum	Maximum
G [GPa]	80	90
ν [-]	0.27	0.31
W_s' [kJ/m ²]	2.0	440
k [MPa]	100	500

Therefore, parameters A and B which are functions of the material properties can vary according to Table 2.

Table 2
Ranges of material constants.

Parameter	Minimum	Maximum
A [N ² /m ³]	5.9×10^{14}	1.4×10^{17}
B [Pa]	2.0×10^8	1.0×10^9

The number of cycles required to initiate a fatigue crack depends on two variables: the length of the persistent slip band d (which can be approximate to the grain size) and the shear stress range $\Delta\tau$.

Equation 2 can be transformed in order to give $\Delta\tau$ as a function of N_i and then to plot a S-N curve that gives the shear stress range required to initiate a crack for a certain number of cycles.

$$\Delta\tau = B + \sqrt{\frac{A}{dN_i}} \quad (5)$$

Figure 1 shows the influence of material constants A and B on the S-N fatigue crack initiation curve for an average grain size of $25 \mu\text{m}$ (which corresponds to a standard bearing steel).

The dashed lines correspond to the lower and upper bounds using respectively the most critical A and B values while the colored curves only show the influence of one parameter by setting the second to an intermediate value.

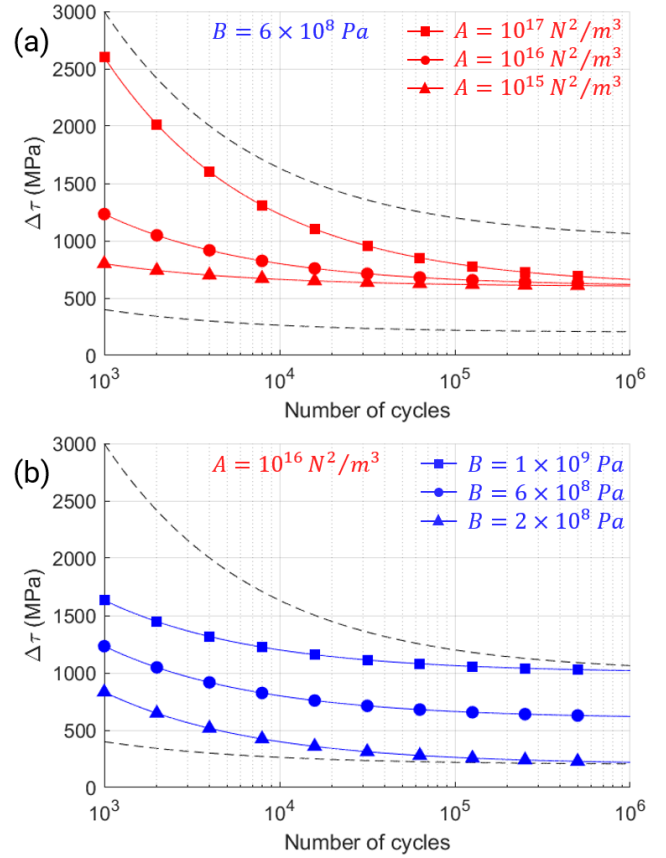


Figure 1: S-N curves depending on (a) variation of material constant A and (b) variation of material constant B .

A has more influence at low-cycle fatigue. This parameter is related to rigidity and fracture energy of the material. A larger A corresponds to a material that is strongly resistant to fatigue crack initiation.

B acts as a threshold parameter. If the shear stress range $\Delta\tau$ does not overcome B , the fatigue crack threshold N_i is infinite. Indeed, this constant is directly correlated to the frictional stress k which is the resistance that a dislocation needs to overcome in order to move.

In order to implement this fatigue model into a numerical RCF model, shear stress range needs to be calculated. In this study two approaches are compared: macroscopic and mesoscopic.

3. Macroscopic modeling

3.1. Model

The model is designed to represent a contact between two bodies in 2D. Only one of the bodies is modeled. The action of the second one is emulated by a moving contact pressure. This method is commonly used in the literature [24, 41, 42, 21].

Hertz contact theory [43] provides tools to calculate the pressure field in contacts. The contact pressure distribution $p(x)$, the half-width of the contact area a and the maximum contact pressure p_0 are described by Johnson [44].

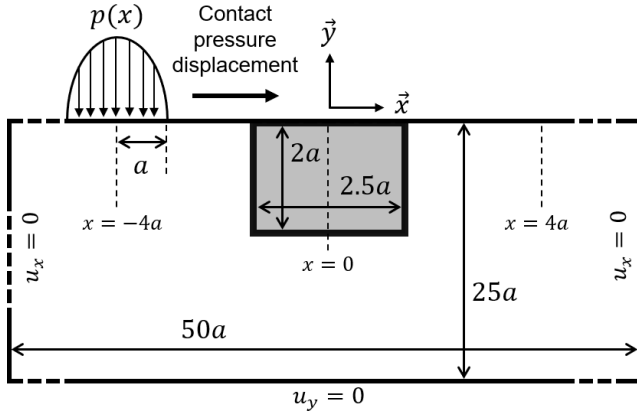


Figure 2: Model dimensions and contact pressure position.

The objective is to obtain the stress distribution in the material. In order to be computationally efficient, there is no need for a high level of accuracy in a very large area, only the area of stress concentration is of interest. Generally, in the case of a Hertzian contact, the area of maximum stress is between the surface and a depth of $2a$. In the direction of the contact pressure displacement, $2.5a$ was found to be sufficient to cover the width to the stress concentration. Ideally, this area of analysis of $2a \times 2.5a$ at the surface would be embedded into a semi-infinite body so that there is no effect of the boundary conditions on the stress field. With fixed perpendicular displacements at the left, right and bottom edges, a body of dimension $50a \times 25a$ is equivalent to a semi-infinite body (the stress difference being negligible) [45]. Figure 2 shows model dimensions, boundary conditions and moving contact pressure positions.

The relative displacement of the bodies is modeled by the incremental displacement of the contact pressure from its initial position to its final position at each calculation step. The initial position is set to $x_0 = -4a$ for the center of the contact pressure field and its final position is set to $x_f = 4a$.

This loading condition is representative for perfectly smooth linear contact [44]. In RCF, surface roughness, manufacturing defects, dents caused by particle contamination or EHL lubrication strongly affect the standard Hertz contact pressure. These factors can introduce stress concentrations in the material and thus, modify the location of the critical areas [44]. Nowadays, it is well accepted that considering surface fatigue, for rolling bearing applications, surface roughness of the components being generally low, dents appear to be more severe [46, 47, 48]. Whereas, for gear applications, as surface roughness is important compared to film thickness, it can be the predominant driver of fatigue failure. To emphasize the impact of surface defects compared to smooth surfaces, the authors choose to consider dents in this study. However, similar analyses considering surface roughness are possible.

Coulon et al. characterized dent geometry with three parameters: dent diameter ϕ , dent depth d_{th} and shoulder height is determined by K [46]. The shape function of a

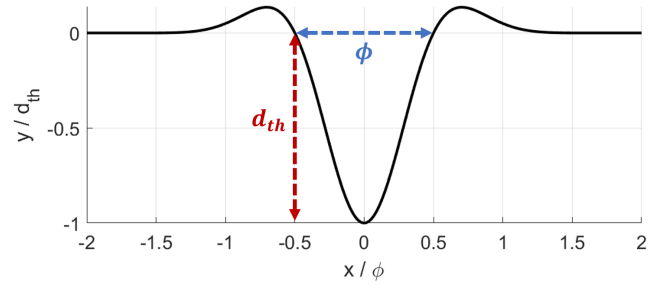


Figure 3: Analytical dent shape and parameters.

dent on the (x, z) plane is:

$$f(x, z) = -d_{th} \exp\left(-K \frac{x^2 + z^2}{4\phi^2}\right) \cos\left(\pi \frac{\sqrt{x^2 + z^2}}{\phi}\right) \quad (6)$$

Since the model is two-dimensional, the dent shape is considered as the section of the shape function at $z = 0$. Figure 3 illustrates the resulting 2D dent shape.

As a comparison between a perfectly smooth surface and a more critical case, the simulation is performed with both loading conditions.

- Hertzian contact: $p = p_{hertz}$
- Dented contact: $p = p_{hertz} + \Delta p_{dent}$

Δp_{dent} has been determined by Coulon et al. [46, 47] depending on the dent characteristics. Half-width of the contact a , maximum contact pressure p_0 and dent characteristics used in this study are described in Table 3. Dent is symmetric and is considered to be centered at $x = 0$.

Table 3
Contact and dent characteristics.

Characteristic	Value
Half-width a [μm]	615
Max contact pressure p_0 [MPa]	2100
Dent diameter ϕ [μm]	250
Dent depth d_{th} [μm]	37
Dent shoulder parameter K [-]	12

The contact pressure of the two loading cases are shown in Figure 4, the darker area represents the coordinates of the area of analysis.

Stress components σ_x , σ_y , σ_z and τ_{xy} are obtained by FEM computation with plane deformation assumptions. Stress tensor is calculated for each incremental position of the moving contact pressure with quasi-static conditions. The simulation is performed for dry contact, in order to analyze the most severe case of damage [46].

FEM analysis is performed with isotropic and homogeneous material properties. The values that are used in this study are shown in Table 4.

Mesh size has been adapted to be fine in regions of high stress gradient (near dent), coarser in region of lower stress

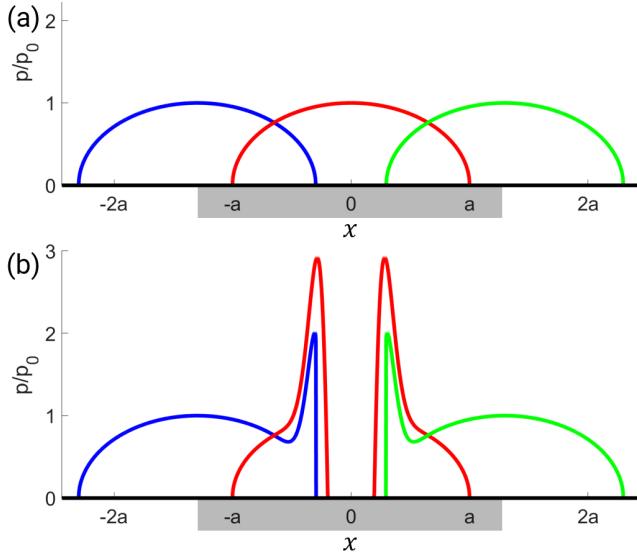


Figure 4: Contact pressure for load centered on (blue) $x = -1.3a$, (red) $x = 0$, (green) $x = 1.3a$, for (a) Hertzian contact (b) dented contact.

Table 4

Material properties of the simulation.

Property	Value
Young's modulus E [GPa]	200
Poisson's ratio ν [-]	0.3

gradient and a lot coarser outside the area of analysis. Therefore, element size is set to:

- $5\mu\text{m}$ between a depth of 0 and $0.5a$ inside the area of analysis,
- $10\mu\text{m}$ between a depth of $0.5a$ and $2.5a$ inside the area of analysis,
- Progressive element size between edges of the area of analysis and left, right and bottom edges of wide body where element size is prescribed to 5mm .

Mesh sensitivity has been assessed to suppress mesh dependency. The mesh is the same for both smooth and dented surfaces.

3.2. Shear stress

The Tanaka-Mura model was originally intended for uniaxial tensile fatigue. In the case of uniaxial loading, the shear stress is maximized for the directions at 45° from the loading direction.

In rolling contact fatigue, the loading is multi-axial, therefore, several approaches can be considered. At least three different critical shear stresses have been used in different RCF models [20]:

- Orthogonal xy shear stress τ_{xy} [29]
- Maximum shear stress τ_{max} [49]
- Octahedral shear stress τ_{oct} [18]

In this study, a rotation of 45° of the stress tensor is performed since this is the direction that maximizes τ_{max} for a Hertzian contact.

τ_{xy} is directly computed by the FEM simulation, τ_{45} can be deduced by rotation, τ_{max} and τ_{oct} are obtained using the principal coordinate system.

In continuum mechanics, the stress tensor can be diagonalized when expressed in the principal coordinate system.

Maximum shear stress τ_{max} (also known as Tresca shear stress) is defined by:

$$\tau_{max} = \frac{1}{2}(\sigma_I - \sigma_{III}) \quad (7)$$

With σ_I and σ_{III} , the maximum and the minimum principal stresses ($\sigma_I \geq \sigma_{II} \geq \sigma_{III}$). τ_{max} is oriented according to the bisector of the 1st and the 3rd principal directions.

Octahedral shear stress τ_{oct} is defined by:

$$\tau_{oct} = \frac{1}{3} \sqrt{(\sigma_I - \sigma_{II})^2 + (\sigma_{II} - \sigma_{III})^2 + (\sigma_{III} - \sigma_I)^2} \quad (8)$$

τ_{oct} is oriented according to the plane whose normal vector forms equal angles with the three principal directions.

In the case of Hertzian contact pressure, shears maximum values and critical depths are different depending on the shear stress (see Table 5).

Table 5

Max and depth at max of different shear stresses for Hertzian contact [44].

Shear stress	Depth at max	Max
τ_{xy}	$0.50a$	$0.25p_0$
τ_{45}	$0.78a$	$0.30p_0$
τ_{max}	$0.78a$	$0.30p_0$
τ_{oct}	$0.67a$	$0.26p_0$

For dented surfaces, no analytical law provides the critical depths and the maximum values of the different shear stresses. However, these results can be obtained numerically (see Table 6).

Table 6

Max and depth at max of different shear stresses for dented contact.

Shear stress	Depth at max	Max
τ_{xy}	$0.069a$	$0.74p_0$
τ_{45}	$0.078a$	$0.71p_0$
τ_{max}	$0.062a$	$0.78p_0$
τ_{oct}	$0.061a$	$0.70p_0$

Figure 5 shows the different shear stresses for the centered contact pressure. For Hertzian and dented contact cases, stress fields are symmetric (τ_{45} , τ_{max} , τ_{oct}) or antisymmetric (τ_{xy}), therefore, the illustrations are split between both cases.

τ_{max} is the most critical stress for centered static contact pressure, making it a commonly used criterion in fatigue. In the following section, shear stress ranges are calculated for a

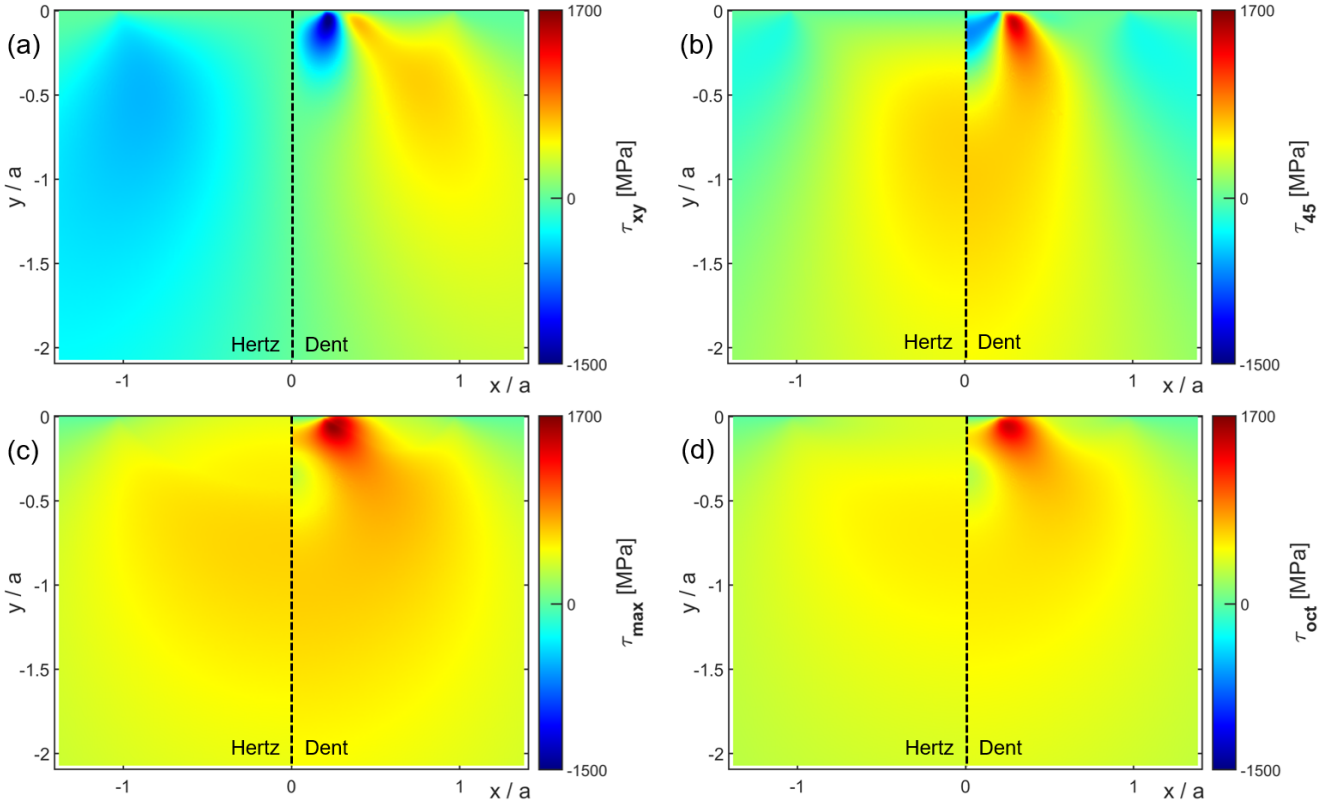


Figure 5: (a) Orthogonal xy shear stress τ_{xy} , (b) orthogonal 45° shear stress τ_{45} , (c) maximum shear stress τ_{max} , (d) octahedral shear stress τ_{oct} ; centered contact pressure.

moving contact pressure to simulate the passing of a contact body.

3.3. Shear stress range

Shear stress range $\Delta\tau$ can be defined as the difference between the maximum and the minimum of shear stress τ during a full stress cycle.

Figure 6 gives the shear stress ranges for the different shears. Since all stress fields are symmetric, the illustrations are split between Hertzian and dented contact cases.

τ_{max} and τ_{oct} depend on the principal coordinate system whose orientation can change at each simulation step (see Figure 7). This is not ideal in the case of a moving contact pressure since neither of $\Delta\tau_{max}$ nor $\Delta\tau_{oct}$ represents the shear stress range on any fixed resolved direction. Moreover, τ_{max} and τ_{oct} are continually positive values which results in smaller ranges than fixed coordinate system shear stresses. For example, $\tau_{max} > \tau_{xy}$ but $\Delta\tau_{max} < \Delta\tau_{xy}$.

For Hertzian contacts, Table 7 gives the depths that maximize the shear stress ranges.

Maximum values and depths of maximum values of shear stresses for the dented contact are given thanks to numerical computations (see Table 8).

It appears in Table 7 and Table 8 that $\Delta\tau_{xy}$ is the most critical shear stress of the four in these configurations. This result is also visible when looking at the variations of the different shear stresses as functions of the contact pressure position (see Figure 8).

Table 7

Max and depth at max of different shear stress ranges for Hertzian contact.

Shear stress range	Depth at max	Max
$\Delta\tau_{xy}$	$0.50a$	$0.50p_0$
$\Delta\tau_{45}$	$0.63a$	$0.37p_0$
$\Delta\tau_{max}$	$0.78a$	$0.30p_0$
$\Delta\tau_{oct}$	$0.67a$	$0.26p_0$

Table 8

Max and depth at max of different shear stress ranges for dented contact.

Shear stress range	Depth at max	Max
$\Delta\tau_{xy}$	$0.021a$	$1.2p_0$
$\Delta\tau_{45}$	$0.068a$	$0.82p_0$
$\Delta\tau_{max}$	$0.061a$	$0.80p_0$
$\Delta\tau_{oct}$	$0.059a$	$0.71p_0$

Maximum and octahedral shears are two critical stresses that are therefore more relevant in case of repeated static pressure. For contact fatigue where the pressure is moving, fixed coordinate system critical stresses should be privileged. This is the case of $\Delta\tau_{xy}$ and $\Delta\tau_{45}$.

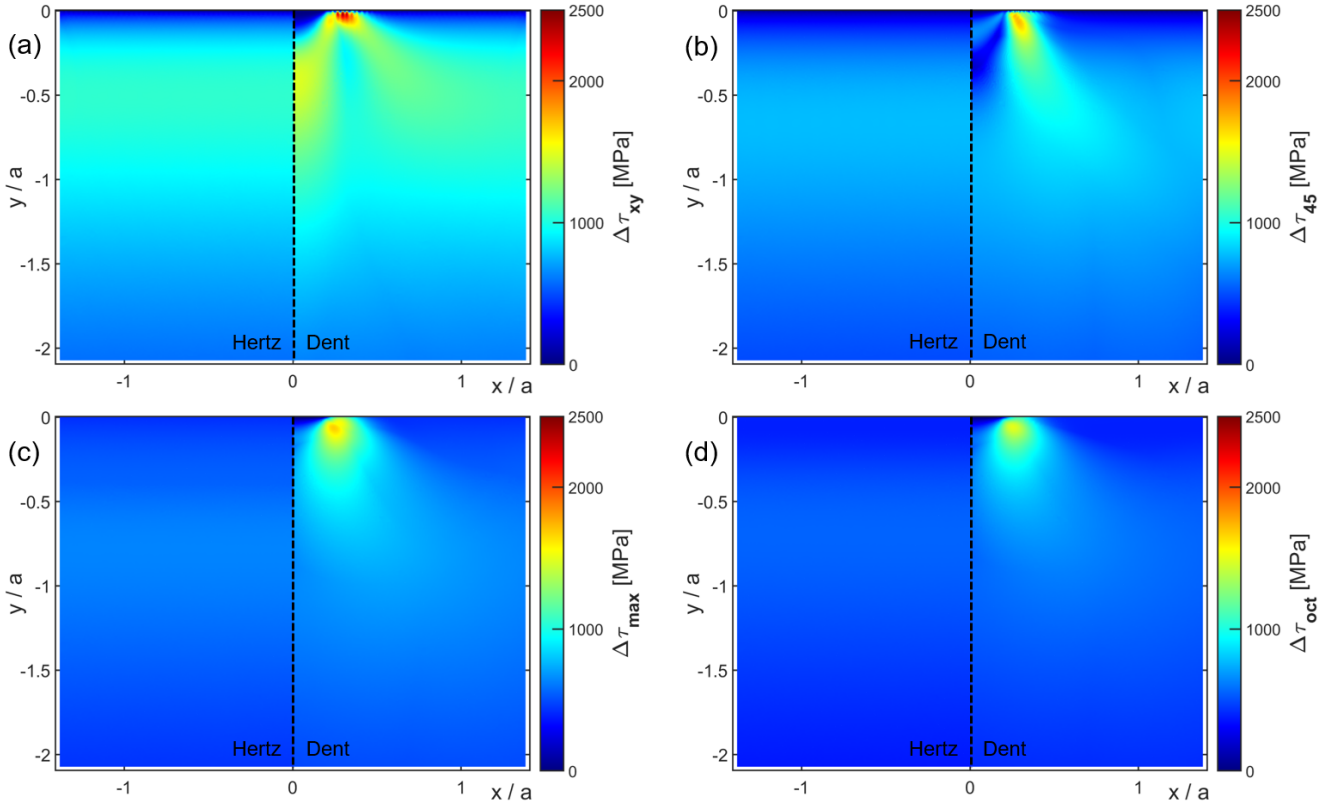


Figure 6: (a) Orthogonal xy shear stress range $\Delta\tau_{xy}$, (b) orthogonal 45° shear stress range $\Delta\tau_{45}$, (c) maximum shear stress range $\Delta\tau_{max}$, (d) octahedral shear stress range $\Delta\tau_{oct}$.

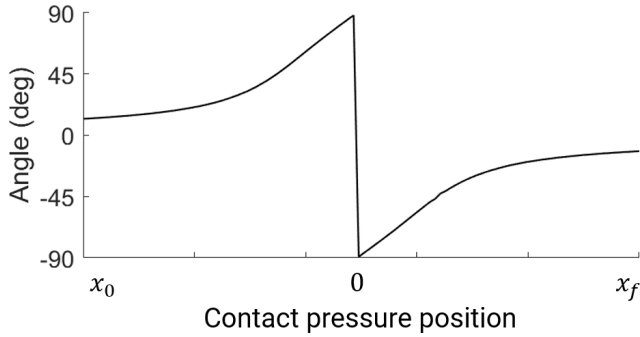


Figure 7: Principal coordinate system orientation relative to xy fixed coordinate system at $x = 0$ and $y = -0.78a$.

3.4. Fatigue crack threshold

Figure 9 shows the number of cycles N_i resulting from the Tanaka-Mura (Equation 2) using four different stresses. These results are obtained using the parameters given Table 9.

Table 9
Macroscopic approach parameters.

Parameter	Value
A [N^2/m^3]	1.28×10^{17}
B [Pa]	7.8×10^8
d [μm]	25

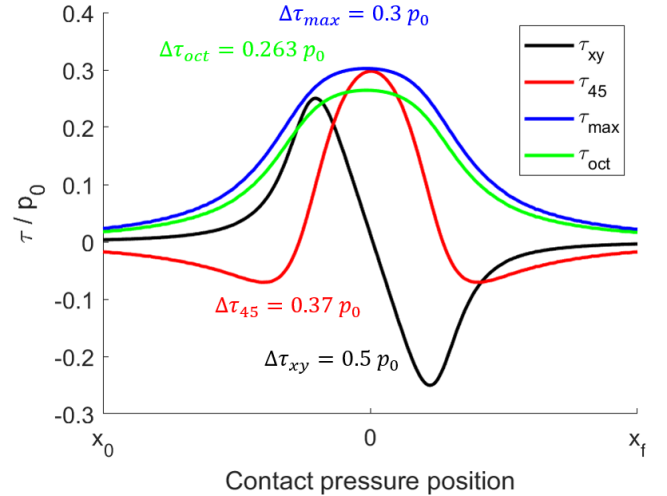


Figure 8: Variation of the different shear stresses for Hertzian contact at $x = 0$ and $y = -depth_{max}$.

In the case of Hertzian contact pressure, the use of $\Delta\tau_{xy}$ gives the critical results (smaller $N_{i,min}$). The nondestructive testing by Yoshioka showed that cracks first initiate at the depth of the maximum of $\Delta\tau_{xy}$ [50]. These results were also found in tests by Chen et al. [51, 52]. These observations confirmed that $\Delta\tau_{xy}$ is more critical than $\Delta\tau_{45}$ in the case of a smooth surface.

The slip band length d is considered as a constant, rep-

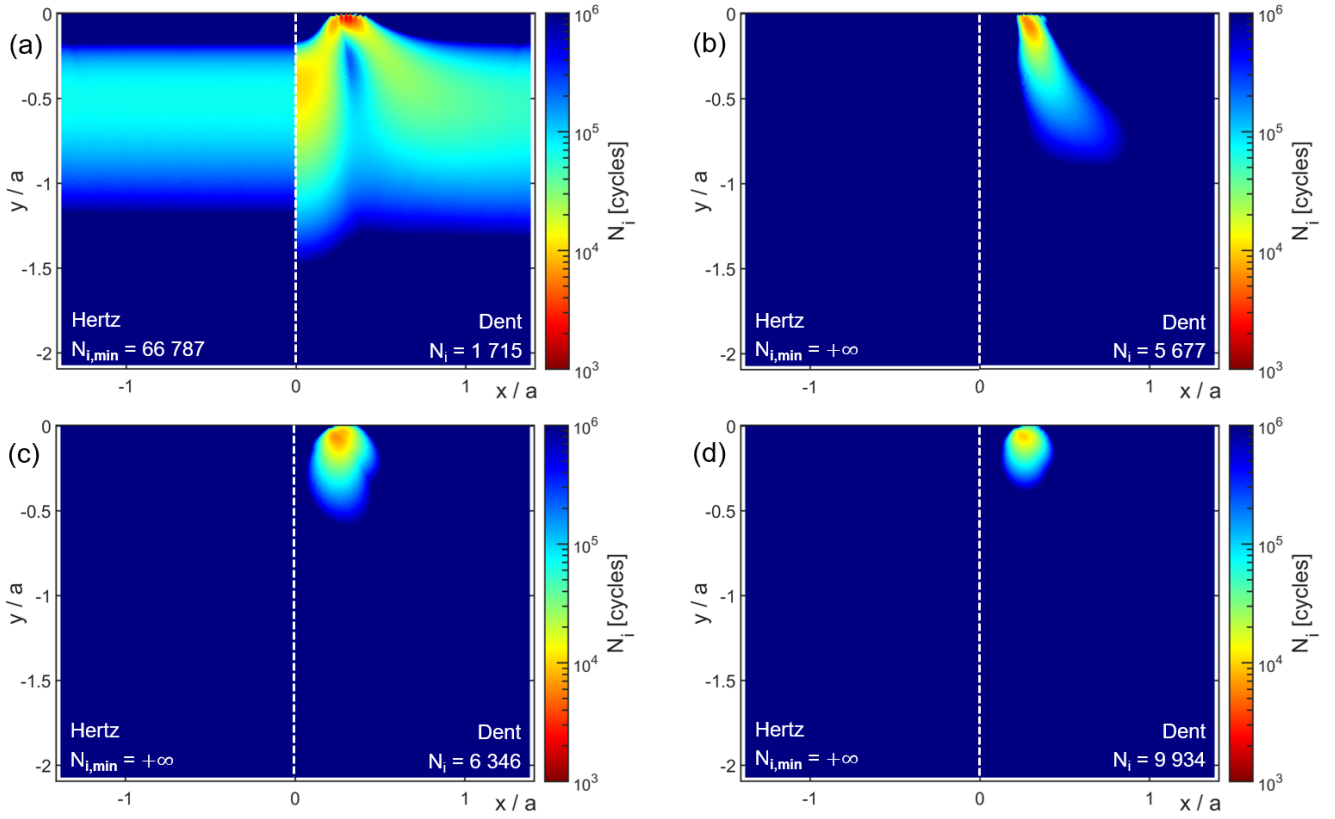


Figure 9: Number of cycles for crack initiation using (a) $\Delta\tau_{xy}$, (b) $\Delta\tau_{45}$, (c) $\Delta\tau_{max}$, (d) $\Delta\tau_{oct}$.

representative for the mean grain size. This assumption can be questioned as in a real material, some of the grains are larger than the mean grain size, and some others are smaller. This distribution has a direct effect on fatigue crack threshold.

Surface defects such as a dent cause contact pressure to increase and consequently alterations in the stress field. As Figure 9 shows, the presence of a dent induces a variation of $N_{i,min}$ but also a variation of the spatial distribution. The comparison between multiple shear stresses have shown that τ_{xy} is more relevant than τ_{45} . However, the orientation that maximize $\Delta\tau$ could be different than 0° and 45° . Moreover, this orientation could vary depending on the position in the material.

The use of a polycrystalline geometry would open opportunities of improvement concerning the calculation of both the shear stress range $\Delta\tau$ and the PSB length d . Different shear stress directions could be calculated for each grain and an algorithm could even optimize these directions in order to consider the most critical cases. The distribution of slip band length d would be much more representative of a real material as long as the polycrystalline geometry is realistic.

4. Mesoscopic modeling

The mesoscopic approach is similar to the macroscopic approach except for the area of analysis (see Figure 2) which is replaced by a granular geometry. The geometry of this area is generated with Neper [53, 54, 55]. It uses Voronoi's

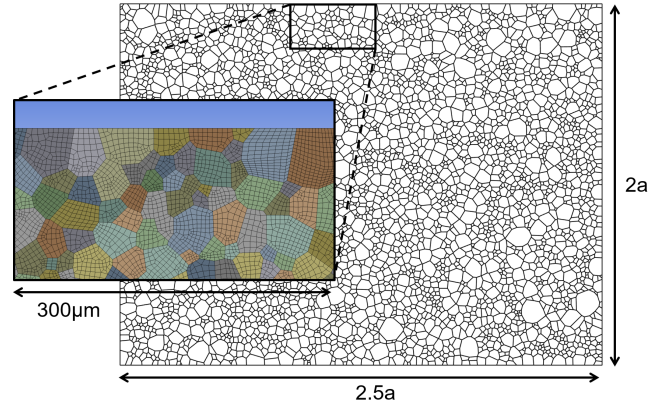


Figure 10: Polycrystalline geometry used for the area of analysis (generated with Neper [53, 54, 55]).

tessellations to generate polycrystalline geometry. Grain sizes follow a log-normal distribution with a mean value of $25\mu m$ and a standard deviation of $11\mu m$ (see Figure 10). Each grain is meshed into quadrangle quadratic elements.

4.1. Shear stress range

In this study, mesoscopic shear stress is the shear stress calculated in the fixed direction that maximizes the shear stress range $\Delta\tau$ for each grain. Only in-plane shear is considered. The mesoscopic shear stress range $\Delta\tau_{meso}$ is obtained by an algorithm which tests every resolved direction

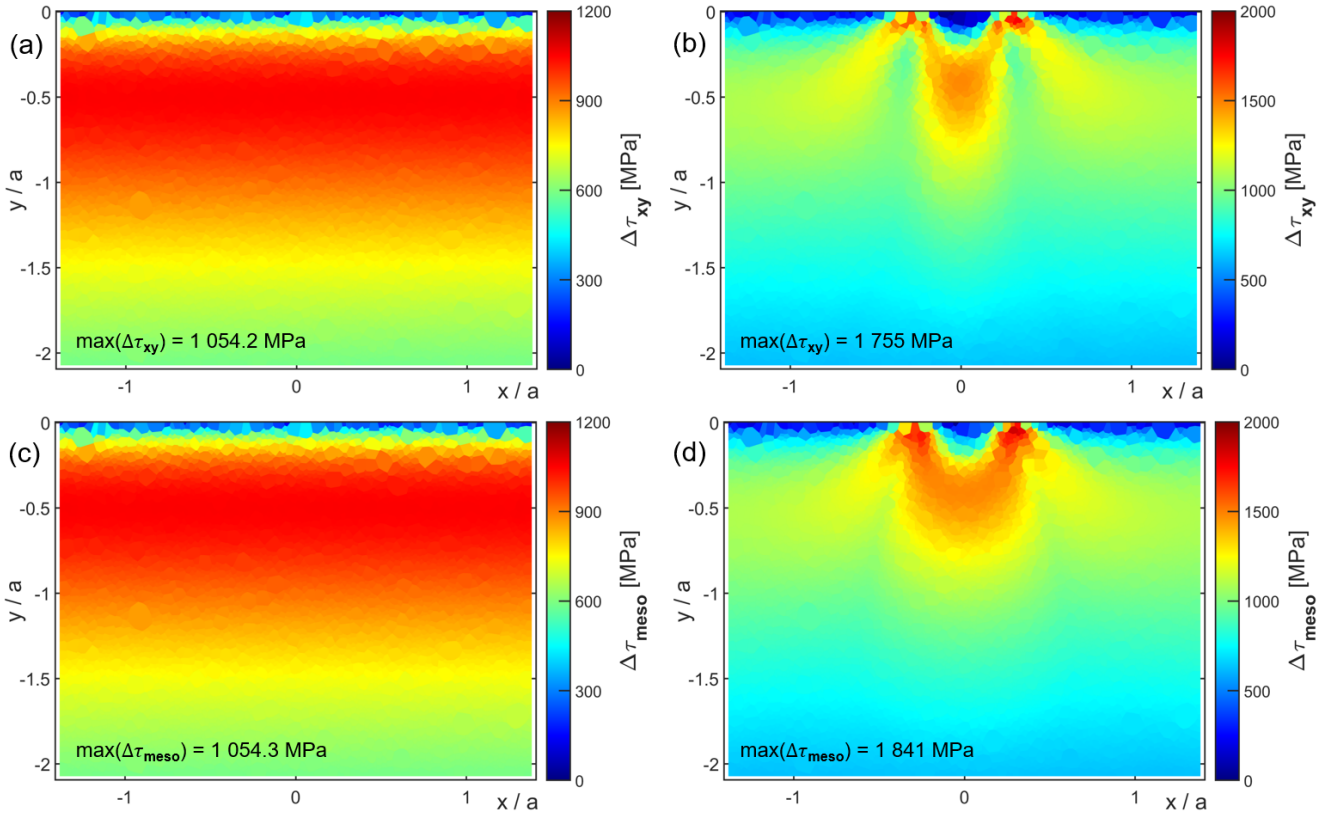


Figure 11: Comparison between (a,b) orthogonal shear stress range $\Delta\tau_{xy}$ and (c,d) mesoscopic resolved shear stress range $\Delta\tau_{meso}$ for (a,c) hertzian contact pressure and (b,d) dented surface.

from 0° to 90° with an angular increment of 0.1° . For each grain, the algorithm keeps the direction that maximized the shear stress range. The four components σ_x , σ_y , σ_z and τ_{xy} of each element of a grain are averaged to give mean values for each grain. The following results are all grain-related values in opposition of section 3 where the results were element-related values.

The main advantage of the mesoscopic method is that the direction of $\Delta\tau$ corresponds to the most favorable orientation for dislocation slip is ensured. In the case of the Hertzian contact (Figure 11), there is no significant difference between (a) $\Delta\tau_{xy}$ and (c) $\Delta\tau_{meso}$ because xy coordinate system is already favorable for maximization of $\Delta\tau$. It confirms that orthogonal xy shear is relevant in smooth surface cases.

However, there is a 5% difference between the maximum of $\Delta\tau_{xy}$ and the maximum of $\Delta\tau_{meso}$ in a dented surface (see Figure 11 (b, d)). Mesoscopic method is more critical than the uniform resolved direction and stress field distribution is different. High stress concentration zone covers a larger area in case of mesoscopic method, in contrast with $\Delta\tau_{xy}$ where concentration region is smaller.

Orthogonal shear stress is commonly used for RCF, this comparison with mesoscopic shear stress shows that it is valid in case of Hertzian contact, however, results with a dented surface illustrate that it could be less legitimate in other cases.

4.2. Fatigue crack threshold

Fatigue crack threshold is computed thanks to Tanaka-Mura equation (see Equation 2). Same material constants A and B than the macroscopic approach are used (Table 9). Shear stress range $\Delta\tau$ calculation is detailed in the previous section and d is computed using the granular geometry. For each grain, d is the length of the longest segment calculated in the direction of $\Delta\tau_{meso}$. In Hertzian contact, the value of $\Delta\tau$ is constant for a given depth, therefore, the variation of N_i at constant depth is exclusively due to grain size variations.

Figure 12 shows fatigue crack threshold results obtained in polycrystalline geometry using three different methods. (a) and (b) show the results for a static centered contact pressure and the use of τ_{max} , (c) and (d) show the results for a moving contact pressure and the use of orthogonal shear stress range $\Delta\tau_{xy}$, and (e) and (f) shows the results for a moving contact pressure and the use of mesoscopic shear stress range $\Delta\tau_{meso}$.

For the Hertzian contact, the minimum of the number of cycles $N_{i,min}$ is 24082 cycles while it is only 3563 for the dented contact with the mesoscopic approach. As expected, surface conditions have a predominant influence on fatigue crack threshold. A damaged surface will highly decrease N_i .

Computation with moving contact pressure is significantly heavier in terms of CPU time than a simple static contact pressure due to the requirement of numerous calculation steps.

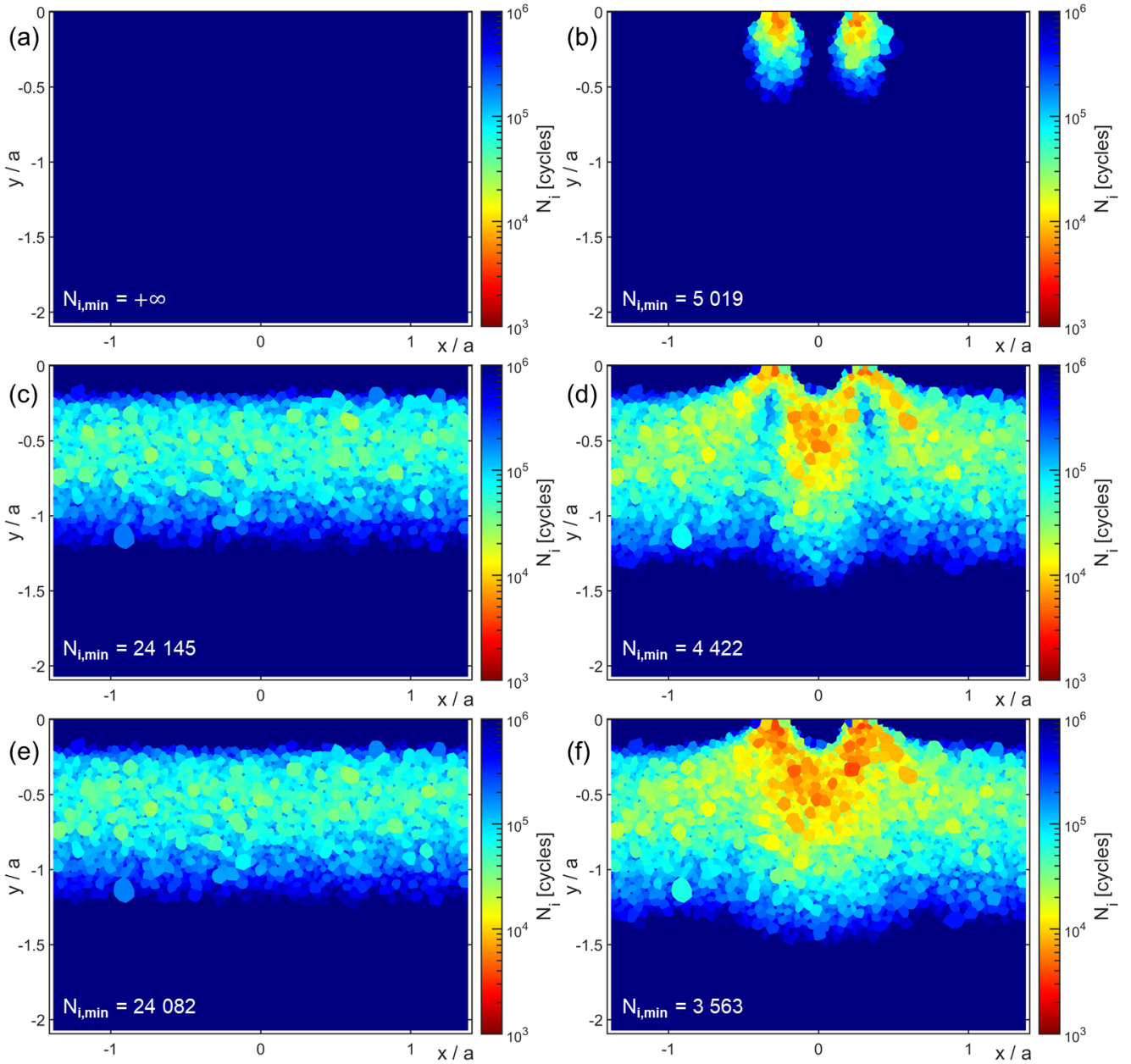


Figure 12: Number of cycles required to initiate fatigue crack for (a,b) static load using τ_{max} , (c,d) moving contact pressure using $\Delta\tau_{xy}$, (e,f) moving contact pressure using $\Delta\tau_{meso}$, (a,c,e) Hertzian contact pressure and (b,d,f) dented contact pressure.

Therefore, the benefit of the moving contact pressure compared to a static pressure can be questioned. Indeed, it is possible to determine $\Delta\tau$ simply by considering the stressed state (static centered contact pressure for example) and a relaxed state (stresses are nil). Repeated stress cycles correspond to alternations between the two states. It turns out that the static contact pressure is not suitable to approximate a rolling contact since the results obtained with the moving contact pressure are significantly different.

Critical initiation depths can be identified Figure 12. The benefit of modeling a polycrystalline geometry is that it introduces a probabilistic aspect of crack initiation. For the Hertzian contact, the combination of $\Delta\tau$ and d distributions results in a depth range where cracks are more likely to first

initiate. Using a threshold of $N_{i,c} = 10 \times N_{i,min}$, this depth ranges from $y = -1.1a$ to $y = -0.2a$. This range is consistent with the experimental observations [51, 52]. Concerning the dented contact, cracks first appear under the dent. The critical depth range varies from $y = -1.0a$ to $y = 0$ (using $N_{i,c} = 10 \times N_{i,min}$). This implies that damaged surfaces tend to originate at smaller depths and eventually at the surface itself.

Concerning the choice of the method used to calculate $\Delta\tau$, it should be noted that in Hertzian contact $N_{i,min}$ is 0.3% higher using $\Delta\tau_{xy}$ than using $\Delta\tau_{meso}$. For the dented contact, $N_{i,min}$ is 24.1% higher using $\Delta\tau_{xy}$ than using $\Delta\tau_{meso}$. This confirms that orthogonal shear is suitable in smooth surface contact. In the case of damaged surfaces that induce less uni-

form contact pressure, the mesoscopic shear stress is more relevant and will provide more critical results.

5. Conclusions

The numerical model for rolling contact fatigue which is presented in this study leads to several conclusions. (1) Modeling the motion of the contact pressure gives significantly different results compared to a static pressure which can imply that static pressure is not relevant to model crack initiation in rolling contact fatigue. (2) The orthogonal xy shear stress is a relevant indicator of the resolved shear stress for most favorable orientations in smooth surface cases. (3) A mesoscopic approach should be preferred in rough or damaged surface cases. The resolved direction of each grain is the one that maximizes $\Delta\tau$. (4) In Hertzian contact cases, cracks first initiate at the depth of maximum orthogonal shear stress of $y = -0.5a$. (5) In damaged surface cases, cracks first initiate at smaller depth values and eventually surface itself.

Even though material properties are actually a drawback to obtain accurate results, the modeling can replicate the physics of fatigue crack initiation and show the most critical locations in different cases. It may be useful for engineers to know the depth at which a surface treatment of the material is beneficial. However, the model described in this article does not replicate all the physics involved in fatigue crack initiation. Firstly, the material model is assumed as homogeneous and isotropic. However, polycrystalline materials present anisotropic characteristics. Anisotropic simulation would allow to model the slip bands that form inside the polycrystalline material. Indeed, intra-granular and inter-granular slip bands are the physical phenomena that led Tanaka and Mura to develop their equation. Although slip band length d is approximated by the grain size in this study, the modeling of the PSB field would provide more physically based results. All these phenomena are as many interesting aspects to pursue in order to try to approach a better modeling of crack initiation.

References

- [1] A. Wöhler, *Über die festigkeitsversuche mit eisen und stahl*. Ernst & Korn, 1870.
- [2] O. H. Basquin, "The exponential law of endurance tests," *Proc Am Soc Test Mater*, vol. 10, pp. 625–630, 1910.
- [3] A. G. Palmgren, "Die lebensdauer von kugellagern," *Zeitschrift des Vereinesdeutscher Ingenieure*, vol. 68, no. 14, pp. 339–341, 1924.
- [4] E. Wilkins, "Cumulative damage in fatigue," in *Colloquium on Fatigue/Colloque de Fatigue/Kolloquium über Ermüdungsfestigkeit*, pp. 321–332, Springer, 1956.
- [5] L. F. Coffin, "A study of the effects of cyclic thermal stresses on a ductile metal," *Transactions of the American Society of Mechanical Engineers, New York*, vol. 76, pp. 931–950, 1954.
- [6] S. S. Manson, *Behavior of materials under conditions of thermal stress*, vol. 2933. National Advisory Committee for Aeronautics, 1953.
- [7] A. V. Olver, "The mechanism of rolling contact fatigue: An update," *Proceedings of the Institution of Mechanical Engineers, Part J: Journal of Engineering Tribology*, vol. 219, no. 5, pp. 313–330, 2005.
- [8] F. Sadeghi, B. Jalalahmadi, T. S. Slack, N. Raje, and N. K. Arakere, "A Review of Rolling Contact Fatigue," *Journal of Tribology*, vol. 131, 09 2009. 041403.
- [9] M. Klesnil and P. Lukác, *Fatigue of metallic materials*, vol. 71. Elsevier, 1992.
- [10] M. D. Sangid, H. J. Maier, and H. Sehitoglu, "A physically based fatigue model for prediction of crack initiation from persistent slip bands in polycrystals," *Acta Materialia*, vol. 59, no. 1, pp. 328 – 341, 2011.
- [11] K. Tanaka and T. Mura, "A Dislocation Model for Fatigue Crack Initiation," *Journal of Applied Mechanics*, vol. 48, pp. 97–103, 03 1981.
- [12] A. Brückner-Foit and X. Huang, "Numerical simulation of microcrack initiation of martensitic steel under fatigue loading," *International Journal of Fatigue*, vol. 28, no. 9, pp. 963 – 971, 2006. Fatigue lifetime prediction of metals based on microstructural behaviour.
- [13] A. Bruckner-Foit and X. Huang, "On the determination of material parameters in crack initiation laws," *Fatigue & Fracture of Engineering Materials & Structures*, vol. 31, no. 11, pp. 980–988, 2008.
- [14] S. Toyoda, H. Kimura, Y. Kawabata, S. Hashimoto, N. Yoshihara, and J. Sakai, "Numerical simulation of fatigue crack initiation in thin-walled high strength steel as modeled by voronoi-polygons," *ISIJ international*, vol. 50, no. 11, pp. 1695–1701, 2010.
- [15] P.-M. Hilgendorff, A. Grigorescu, M. Zimmermann, C.-P. Fritzen, and H.-J. Christ, "Simulation of irreversible damage accumulation in the very high cycle fatigue (vhcf) regime using the boundary element method," *Materials Science and Engineering: A*, vol. 575, pp. 169 – 176, 2013.
- [16] F. Briffod, T. Shiraiwa, and M. Enoki, "Fatigue crack initiation simulation in pure iron polycrystalline aggregate," *Materials Transactions*, vol. 57, no. 10, pp. 1741–1746, 2016.
- [17] R. S. Zhou, H. S. Cheng, and T. Mura, "Micropitting in Rolling and Sliding Contact Under Mixed Lubrication," *Journal of Tribology*, vol. 111, pp. 605–613, 10 1989.
- [18] R. S. Zhou, "Surface topography and fatigue life of rolling contact bearing," *Tribology Transactions*, vol. 36, no. 3, pp. 329–340, 1993.
- [19] W. Cheng, H. S. Cheng, T. Mura, and L. M. Keer, "Micromechanics Modeling of Crack Initiation Under Contact Fatigue," *Journal of Tribology*, vol. 116, pp. 2–8, 01 1994.
- [20] W. Cheng and H. S. Cheng, "Semi-Analytical Modeling of Crack Initiation Dominant Contact Fatigue Life for Roller Bearings," *Journal of Tribology*, vol. 119, pp. 233–240, 04 1997.
- [21] N. Raje, T. Slack, and F. Sadeghi, "A discrete damage mechanics model for high cycle fatigue in polycrystalline materials subject to rolling contact," *International Journal of Fatigue*, vol. 31, no. 2, pp. 346 – 360, 2009.
- [22] N. R. Paulson, F. Sadeghi, and W. Habchi, "A coupled finite element ehl and continuum damage mechanics model for rolling contact fatigue," *Tribology International*, vol. 107, pp. 173–183, 2017.
- [23] S. J. Lorenz, F. Sadeghi, H. K. Trivedi, L. Rosado, M. S. Kirsch, and C. Wang, "A continuum damage mechanics finite element model for investigating effects of surface roughness on rolling contact fatigue," *International Journal of Fatigue*, vol. 143, p. 105986, 2021.
- [24] E. Bossy, J. Noyel, X. Kleber, F. Ville, C. Sidoroff, and S. Thibault, "Competition between surface and subsurface rolling contact fatigue failures of nitrided parts: A dang van approach," *Tribology International*, vol. 140, p. 105888, 2019.
- [25] M. Cerullo, "Application of dang van criterion to rolling contact fatigue in wind turbine roller bearings under elasto-hydrodynamic lubrication conditions," *Proceedings of the Institution of Mechanical Engineers, Part C: Journal of Mechanical Engineering Science*, vol. 228, no. 12, pp. 2079–2089, 2014.
- [26] W. Wang, H. Liu, C. Zhu, P. Wei, and J. Tang, "Effects of microstructure on rolling contact fatigue of a wind turbine gear based on crystal plasticity modeling," *International Journal of Fatigue*, vol. 120, pp. 73–86, 2019.
- [27] G. E. Morales-Espejel, A. Gabelli, and A. J. C. de Vries, "A model for rolling bearing life with surface and subsurface survival—tribological effects," *Tribology Transactions*, vol. 58, no. 5, pp. 894–906, 2015.
- [28] G. E. Morales-Espejel and A. Gabelli, "A model for gear life with

- surface and subsurface survival: Tribological effects,” *Wear*, vol. 404–405, pp. 133–142, 2018.
- [29] G. Lundberg, “Dynamic capacity of rolling bearings,” *IVA Handlingar*, vol. 196, p. 12, 1947.
- [30] E. Ioannides and T. A. Harris, “A New Fatigue Life Model for Rolling Bearings,” *Journal of Tribology*, vol. 107, pp. 367–377, 07 1985.
- [31] M. D. Sangid, “The physics of fatigue crack initiation,” *International Journal of Fatigue*, vol. 57, pp. 58–72, 2013. Fatigue and Microstructure: A special issue on recent advances.
- [32] T. Mura and Y. Nakasone, “A theory of fatigue crack initiation in solids,” *Journal of Applied Mechanics*, vol. 57, pp. 1–6, 1990.
- [33] T. Mura, “A theory of fatigue crack initiation,” *Materials Science and Engineering: A*, vol. 176, no. 1, pp. 61–70, 1994.
- [34] X. Wu, “A fatigue crack nucleation model for anisotropic materials,” *Fatigue & Fracture of Engineering Materials & Structures*, vol. 42, no. 1, pp. 387–393, 2019.
- [35] K. S. Chan, “A microstructure-based fatigue-crack-initiation model,” *Metallurgical and Materials Transactions A*, vol. 34, no. 1, pp. 43–58, 2003.
- [36] R. Tryon and T. Cruse, “A reliability-based model to predict scatter in fatigue crack nucleation life,” *Fatigue & Fracture of Engineering Materials & Structures*, vol. 21, no. 3, pp. 257–267, 1998.
- [37] E. O. Hall, “The deformation and ageing of mild steel: III discussion of results,” *Proceedings of the Physical Society. Section B*, vol. 64, pp. 747–753, sep 1951.
- [38] N. J. Petch, “The cleavage strength of polycrystals,” *Journal of the Iron and Steel Institute*, vol. 174, pp. 25–28, 1953.
- [39] N. Jezernik, J. Kramberger, T. Lassen, and S. Glodez, “Numerical modelling of fatigue crack initiation and growth of martensitic steels,” *Fatigue & Fracture of Engineering Materials & Structures*, vol. 33, no. 11, pp. 714–723, 2010.
- [40] J. Kramberger, N. Jezernik, P. Göncz, and S. Glodež, “Extension of the tanaka–mura model for fatigue crack initiation in thermally cut martensitic steels,” *Engineering Fracture Mechanics*, vol. 77, no. 11, pp. 2040–2050, 2010. International Conference on Crack Paths 2009.
- [41] J.-P. Noyel, F. Ville, P. Jacquet, A. Gravouil, and C. Changenet, “Development of a granular cohesive model for rolling contact fatigue analysis: Crystal anisotropy modeling,” *Tribology Transactions*, vol. 59, no. 3, pp. 469–479, 2016.
- [42] M. Šraml, J. Flašker, and I. Potrč, “Numerical procedure for predicting the rolling contact fatigue crack initiation,” *International Journal of Fatigue*, vol. 25, no. 7, pp. 585–595, 2003.
- [43] H. R. Hertz, *Über die Berührung fester elastischer Körper und über die Härte*. Universitätsbibliothek Johann Christian Senckenberg, 2006.
- [44] K. Johnson, “Contact mechanics and the wear of metals,” *Wear*, vol. 190, no. 2, pp. 162–170, 1995.
- [45] J.-P. Noyel, *Analyse de l’initiation de fissures en fatigue de contact : Approche mésoscopique*. Theses, INSA de Lyon, Dec. 2015.
- [46] S. Coulon, F. Ville, and A. A. Lubrecht, “Effect of a dent on the pressure distribution in dry point contacts,” *Journal of Tribology*, vol. 124, pp. 220–223, 03 2001.
- [47] S. Coulon, F. Ville, and A. Lubrecht, “An abacus for predicting the rolling contact fatigue life reduction due to debris dents,” in *Boundary and Mixed Lubrication* (D. Dowson, M. Priest, G. Dalmaz, and A. Lubrecht, eds.), vol. 40 of *Tribology Series*, pp. 283–293, Elsevier, 2002.
- [48] S. Coulon, I. Jubault, A. Lubrecht, F. Ville, and P. Vergne, “Pressure profiles measured within lubricated contacts in presence of dented surfaces. comparison with numerical models,” *Tribology International*, vol. 37, no. 2, pp. 111–117, 2004. Austrib 2002.
- [49] E. V. Zaretsky, R. J. Parker, and W. J. Anderson, “A Study of Residual Stress Induced During Rolling,” *Journal of Lubrication Technology*, vol. 91, pp. 314–318, 04 1969.
- [50] T. Yoshioka, “Detection of rolling contact sub-surface fatigue cracks using acoustic emission technique,” *Lubrication Engineering*, vol. 49, pp. 303–308, Apr. 1993.
- [51] L. Chen, Q. Chen, and E. S., “Study on initiation and propagation angles of subsurface cracks in gcr15 bearing steel under rolling contact,” *Wear*, vol. 133, no. 2, pp. 205–218, 1989.
- [52] Q. Chen, E. Shao, D. Zhao, J. Guo, and Z. Fan, “Measurement of the critical size of inclusions initiating contact fatigue cracks and its application in bearing steel,” *Wear*, vol. 147, no. 2, pp. 285–294, 1991.
- [53] R. Quey, P. Dawson, and F. Barbe, “Large-scale 3d random polycrystals for the finite element method: Generation, meshing and remeshing,” *Computer Methods in Applied Mechanics and Engineering*, vol. 200, no. 17, pp. 1729–1745, 2011.
- [54] R. Quey and L. Renversade, “Optimal polyhedral description of 3d polycrystals: Method and application to statistical and synchrotron x-ray diffraction data,” *Computer Methods in Applied Mechanics and Engineering*, vol. 330, pp. 308–333, 2018.
- [55] R. Quey, A. Villani, and C. Maurice, “Nearly uniform sampling of crystal orientations,” *Journal of Applied Crystallography*, vol. 51, pp. 1162–1173, Aug 2018.